Southern Ocean bottom water cooling and ice sheet expansion during the middle Miocene climate transition

Thomas J. Leutert[1,2*], Sevasti Modestou[1,2], Stefano M. Bernasconi[3], A. Nele Meckler[1,2]

[1]Bjerknes Centre for Climate Research, Bergen, 5007, Norway
[2]Department of Earth Science, University of Bergen, Bergen, 5007, Norway
[3]Geological Institute, ETH Zurich, Zurich, 8092, Switzerland

10   [*]Present address: Max Planck Institute for Chemistry, Mainz, 55128, Germany

Correspondence to: Thomas J. Leutert (Thomas.Leutert@mpic.de)

Abstract. The middle Miocene climate transition (MMCT, ~14.5–13.0 Ma) was associated with a significant expansion of Antarctic ice, but the mechanisms triggering the event remain enigmatic. We present a new clumped isotope (Δ_{47}) bottom
15   water temperature (BWT) record from 16.0 Ma to 12.2 Ma from Ocean Drilling Program (ODP) Site 747 in the Southern Ocean, and compare it to existing BWT records. We show that BWTs in the Southern Ocean were ~8–10°C during the middle Miocene greenhouse, and thus considerably warmer than today. Nonetheless, bottom water $\delta^{18}O$ (calculated from foraminiferal $\delta^{18}O$ and Δ_{47}) suggests substantial amounts of land ice throughout the interval of the study. Our dataset demonstrates that BWTs at Site 747 decreased by ~3–5°C across the MMCT. This cooling preceded the stepped main
20   increase in global ice volume, and appears to have been followed by a transient bottom water warming starting during or slightly after the main ice volume increase. We speculate that a regional freshening of the upper water column at this time may have increased stratification and reduced bottom water heat loss to the atmosphere, counteracting global cooling in the bottom waters of the Southern Ocean and possibly even at larger scales. Additional processes and feedbacks required for substantial ice growth may have contributed to the observed decoupling of Southern Ocean BWT and global ice volume.

25   **1 Introduction**

During the Cenozoic Era (the last 65 Myr), Earth's climate transitioned from a state of expansive warmth with very limited ice to colder conditions and permanent ice sheets at the poles (Zachos et al., 2001). The middle Miocene climate transition (MMCT, ~14.5–13 Ma) represents one of the main steps of Cenozoic cooling. A substantial increase in benthic foraminiferal oxygen isotope ratios ($\delta^{18}O$) during the MMCT has been interpreted to reflect a combination of decreasing bottom water
30   temperatures (BWTs) and ice sheet expansion (increasing bottom water $\delta^{18}O$) occurring in the Southern Hemisphere (Lear et al., 2015; Lewis et al., 2007). A roughly coeval decrease in atmospheric pCO_2 of ~100–300 ppm was estimated based on

boron isotope and alkenone records, suggesting a coupling of pCO$_2$ and benthic foraminiferal δ^{18}O during this interval (Sosdian et al., 2018; Super et al., 2018). Atmospheric pCO$_2$ also appears to be coupled to upper ocean temperatures in the North Atlantic and Southern Ocean (Leutert et al., 2020; Super et al., 2018). Conversely, several studies propose a degree of

35 decoupling between BWT and global ice volume during the middle Miocene (Billups and Schrag, 2002; Lear et al., 2010, 2015; Shevenell et al., 2008). These studies are based on deconvolving the bottom water δ^{18}O (δ^{18}O$_{bw}$) and temperature signals in benthic foraminiferal δ^{18}O with independent temperature estimates based on benthic foraminiferal Mg/Ca ratios. Their results indicate a middle Miocene decrease in BWT of ~0.5–3°C. Taking into account the δ^{18}O increase of roughly 1 ‰ in benthic foraminifera, this cooling would imply a drop in global sea level of ~30–110 m, based on the Pleistocene

40 seawater δ^{18}O-sea level calibration of 0.08–0.11 ‰ per 10 m sea level (Fairbanks and Matthews, 1978; Lear et al., 2010) and the oxygen isotope temperature equation (Eq. (9)) of Marchitto et al. (2014). Other approaches using backstripping and different modelling techniques suggest a sea level drop of ~20–40 m across the MMCT (de Boer et al., 2010; Frigola et al., 2018; Kominz et al., 2008; Langebroek et al., 2009).

Although the MMCT represents one of the most fundamental reorganizations in global climate during the Cenozoic era (e.g.,
45 Flower and Kennett, 1993; Zachos et al., 2001), there are still major uncertainties associated with estimating the magnitude and timing of BWT and global ice volume changes. These uncertainties are mainly caused by the small number of independent BWT records resulting in limited spatial and temporal coverage for the middle Miocene, but also by current limitations of the applied temperature proxies. Middle Miocene data coverage is especially poor in the Southern Ocean, where high-resolution BWT records are conspicuously lacking. An existing lower-resolution (~200–300 kyr) Southern

50 Ocean proxy record based on Mg/Ca signatures of benthic foraminiferal tests from Ocean Drilling Program (ODP) Site 747 indicates a bottom water cooling of ~2–3°C from around 15 Ma to 12 Ma (Billups and Schrag, 2002). However, the middle Miocene portion of this BWT record from ODP Site 747 does not have the temporal resolution to adequately capture the magnitude and timing of BWT changes across the MMCT. Furthermore, the application of the Mg/Ca thermometer to middle Miocene benthic foraminifera is complicated by a number of non-thermal effects. Notable amongst these are

55 differential vital effects in foraminifera (e.g., Lear et al., 2002) and the effect of seawater Mg/Ca that has not remained constant on timescales longer than several million years (Evans and Müller, 2012). Finally, benthic foraminiferal Mg/Ca signatures can be influenced by changes in carbonate ion saturation state, especially at low saturation (Elderfield et al., 2006; Lear et al., 2010; Yu and Elderfield, 2008). Previous studies have attempted to minimize saturation state-related effects on Mg/Ca by using only infaunal foraminifera (e.g., *Oridorsalis umbonatus*) precipitating their tests in pore waters that may be

60 buffered to some extent against carbonate saturation changes (Elderfield et al., 2006; Lear et al., 2015) and/or by correcting for changes in saturation state based on paired Mg/Ca and Li/Ca measurements (Lear et al., 2010). Nevertheless, the impact of fluctuating saturation states on middle Miocene Mg/Ca signatures remains controversial. Independent temperature records are required to better understand the mechanisms controlling the Southern Ocean climate evolution during this interval of global change.

65   The carbonate clumped isotope (Δ_{47}) paleothermometer is based on the measured abundance of ^{13}C-^{18}O bonds relative to their stochastic distribution (Ghosh et al., 2006; Schauble et al., 2006), and is independent of the isotopic composition of the parent water from which the carbonate grew (e.g., Eiler, 2011). On the basis of current knowledge, other environmental variables such as pH and salinity appear to be of minor importance for measured Δ_{47} values over the range of natural variation (Tripati et al., 2015; Watkins and Hunt, 2015). When applied to foraminiferal calcite, the method also does not

70   show detectable species-specific vital effects (Grauel et al., 2013; Meinicke et al., 2020; Modestou et al., 2020; Peral et al., 2018; Piasecki et al., 2019; Tripati et al., 2010). Consequently, the Δ_{47} thermometer holds great promise for reconstructing accurate BWTs from benthic foraminiferal tests (e.g., Leutert et al., 2019). The Δ_{47} thermometer has been previously applied to middle Miocene benthic foraminifera from ODP Site 761 in the Indian Ocean yielding results that are in good agreement with Mg/Ca BWTs from the same site (Lear et al., 2010; Modestou et al., 2020). However, there are intervals with very low

75   data density in the middle Miocene record from Site 761, limiting its informative value for understanding the drivers of the MMCT. At the same time, middle Miocene BWTs in other key regions such as the Southern Ocean remain poorly constrained. Here, we present Δ_{47}-based BWTs measured on benthic foraminiferal calcites from ODP Site 747 located on the Kerguelen Plateau in the Southern Ocean (Fig. 1). We compare our new absolute BWT record to previous BWT estimates for the middle Miocene, and interpret the BWT records in the context of middle Miocene glaciation and CO_2 drawdown.

80   ## 2 Material and methods

2.1 Site details

ODP Site 747 (54°48.68'S, 76°47.64'E; 1695 m water depth) lies on the Kerguelen Plateau in the Southern Ocean (Fig. 1; Schlich et al., 1989). At present, the site is situated south of the Polar Front and is bathed by Circumpolar Deep Water (CDW) with a temperature of ~1–2°C (Belkin and Gordon, 1996; Billups and Schrag, 2002). The middle Miocene

85   geographic position of Site 747 relative to Antarctica was similar to today (e.g., Abrajevitch et al., 2014). The clumped isotope record generated in this study covers the depth interval from 62.64 m below sea floor (mbsf, Sample 747A-7H-5, 14-16 cm) to 85.36 mbsf (Sample 747A-9H-8, 75-77 cm) in Hole 747A. 191 samples (15-20 cm^3, mostly calcareous nannofossil ooze with foraminifera) were taken continuously with a mean temporal resolution of ~20 kyr. We slightly rescaled the originally assigned shipboard sample depths to account for core expansion (Schlich et al., 1989), similar to previous studies

90   focusing on the middle Miocene section of Hole 747A (e.g., Abrajevitch et al., 2014; Majewski and Bohaty, 2010).
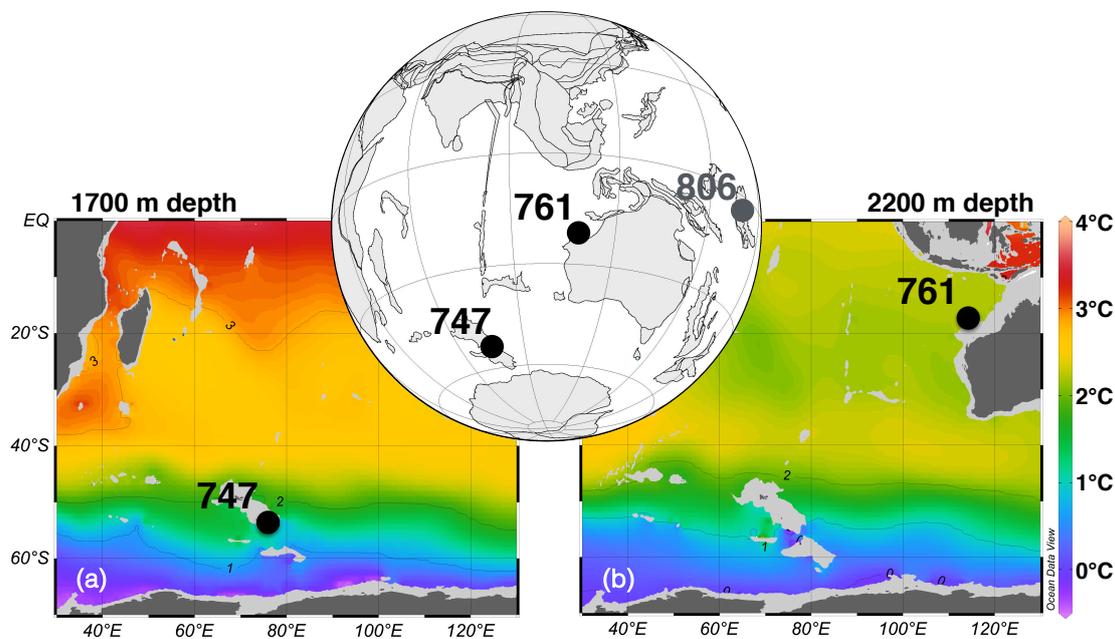
Fig. 1: Ocean temperatures at modern water depths and paleogeographic reconstruction for 14 Ma. Modern water depths of ODP Sites 747 and 761 are ~1700 m and ~2200 m, respectively (Lear et al., 2010; Schlich et al., 1989). Annual mean temperatures at these depths are shown in (**a**) and (**b**). Temperatures from the 2013 World Ocean Atlas (Locarnini et al., 2013) visualized with Ocean Data View (Schlitzer, 2019). Inset map with paleogeographic reconstruction from the plate tectonic reconstruction service of the Ocean Drilling Stratigraphic Network (http://www.odsn.de).

2.2 Sample material

Each sediment sample was freeze-dried, washed over a 63 µm sieve, oven-dried at 50°C and then dry-sieved into different size fractions. We mainly picked tests of *Cibicidoides mundulus* from the 250–355 µm size fraction for our measurements. For samples with low abundances of benthic foraminifera in this size fraction, the >355 µm size fraction was also included. The interval from ~16.0 Ma to ~15.3 Ma was additionally complemented with measurements on *Cibicidoides wuellerstorfi*. Middle Miocene benthic foraminifera (and more specifically *Cibicidoides*) from Site 747 were previously described as well preserved (e.g., Abrajevitch et al., 2014; Billups and Schrag, 2002). Our examination appears to confirm the impression of relatively good preservation of middle Miocene *Cibicidoides* at Site 747 (see Figs. S1 and S2). Similar to other studies (e.g., Billups and Schrag, 2002; Gottschalk et al., 2016; Yu and Elderfield, 2008), *C. mundulus* and *C. wuellerstorfi* are grouped into a single genus. We note that some of the analysed specimens of *C. mundulus* and *C. wuellerstorfi* closely resemble the *sensu lato* morphotype of the respective species (shown in Fig. 2 of Gottschalk et al., 2016).

Prior to isotope analysis, we cracked the picked specimens and ultrasonicated the test fragments in deionized water
110 (3×30 seconds) and methanol (1×10–30 seconds) to remove adhering sediment. Test fragments were rinsed once between
each ultrasonication step and at least three times at the end of the cleaning. The cleaned test fragments were subsequently
oven-dried at 50°C.

2.3 Stable isotope measurements and data processing

Low abundances of carbonate ions containing both ^{13}C and ^{18}O isotopes require stringent analytical procedures and
115 comparably large sample sizes to obtain clumped isotope temperatures that are precise enough for Cenozoic ocean
temperature reconstructions. We achieve the necessary precision by averaging over ~30–40 clumped isotope values
measured on small (~100 μg) carbonate samples (Fernandez et al., 2017; Hu et al., 2014; Meckler et al., 2014; Schmid and
Bernasconi, 2010). Results from adjacent samples are pooled to achieve this number of measurements (e.g., Grauel et al.,
2013; Rodríguez-Sanz et al., 2017), due to the generally low abundance of mono-specific benthic foraminifera (allowing for
120 only 1–5 individual measurements per sample, Fig. S3b). Producing a low-resolution clumped isotope temperature record
with this approach yields higher-resolution $\delta^{18}O$ and $\delta^{13}C$ time series in parallel.

Clumped isotope measurements were performed using two Thermo Scientific MAT 253 Plus mass spectrometers at the
University of Bergen, Norway, and one Thermo Scientific MAT 253 mass spectrometer at ETH Zurich, Switzerland. All
mass spectrometers were coupled to Thermo Fisher Scientific Kiel IV carbonate preparation devices. CO_2 gas was extracted
125 from a carbonate sample with phosphoric acid at a reaction temperature of 70°C, as reported in Schmid et al. (2012). A
Porapak trap included in each Kiel IV carbonate preparation system was kept at -20°C to remove organic contaminants from
the sample gas (Schmid et al., 2012). Between each run, the Porapak trap was baked out at 120°C for at least one hour for
cleaning. Every measurement run included a similar number of samples and carbonate standards. Four carbonate standards
(ETH-1, ETH-2, ETH-3 and ETH-4) with different isotopic compositions and ordering states were used for monitoring and
130 correction of the results (see Appendix A for details). External reproducibilities (one standard deviation) in corrected
Δ_{47} values of ETH-1, ETH-2, ETH-3 and ETH-4 were typically between 0.030 ‰ and 0.040 ‰ (Table S2). External
reproducibilities (one standard deviation) for $\delta^{18}O$ and $\delta^{13}C$ values of the same standards (given relative to VPDB) were
0.03–0.10 ‰ and 0.02–0.06 ‰, respectively.

We converted the sample Δ_{47} values (averages over ~30–40 separate measurements each) into temperature using a
135 calibration based on various recent datasets from core top-derived foraminifera, corrected with the same carbonate standards
as used in our study (Eq. (2) of Meinicke et al. (2020)):

$$T\ (°C) = \sqrt{\frac{0.0431 \times 10^6}{\Delta_{47} - 0.1876}} - 273.15 \qquad (1)$$

140   This combined calibration has been recommended for foraminifer samples (Meinicke et al., 2020). We note that the individual datasets in this compilation (Meinicke et al., 2020; Peral et al., 2018; Piasecki et al., 2019) are all in good agreement with a travertine-based calibration (Kele et al. (2015), recalculated by Bernasconi et al. (2018)) spanning a wider temperature range (6–95°C). For consistency, previously published Δ_{47}-based ocean temperatures from ODP Sites 761 (Modestou et al., 2020) and 1171 (Leutert et al., 2020) originally based on the travertine calibration were recalculated with

145   the calibration equation of Meinicke et al. (2020). We propagated analytical and calibration uncertainties in Δ_{47}-based temperatures (as described in the supporting information of Huntington et al. (2009)), and report combined uncertainties as 68 % and 95 % confidence intervals. Δ_{47}-based temperatures were used in combination with benthic foraminiferal $\delta^{18}O$ values to calculate $\delta^{18}O_{bw}$ (reported relative to VSMOW) with Eq. (9) of Marchitto et al. (2014).

2.4 Age models

150   We revised the Hole 747A age model by integrating six magnetostratigraphic tie points (Abrajevitch et al., 2014; Majewski and Bohaty, 2010) on the GTS2012 timescale (Gradstein et al., 2012), three benthic foraminiferal $\delta^{13}C$-based tie points associated with the "Monterey" carbon-isotope excursion (using the nomenclature of Holbourn et al. (2007)), and one peak warm event visible in benthic foraminiferal $\delta^{13}C$ and $\delta^{18}O$ (Kochhann et al., 2016) (Table S1). For the $\delta^{13}C$-based tie points, we used the high-resolution isotope stratigraphies of IODP Sites U1335, U1337 and U1338 in the eastern equatorial Pacific

155   Ocean (Holbourn et al., 2014; Kochhann et al., 2016) as reference (Fig. 2c). In addition, we included a hiatus at the core break between Cores 7H and 8H, identified by previous studies (e.g., Majewski and Bohaty, 2010). $\delta^{18}O$ and $\delta^{13}C$ time series of Sites 747, 761, 806, U1335, U1337 and U1338 are shown in Fig. 2 with isotope-based age tie points for Site 747 as black crosses. The age model for Site 761 is from Leutert et al. (2020). For Site 806, we utilized a previously published orbitally tuned age model from ~14.1 Ma to ~13.3 Ma (Holbourn et al., 2013); ages for the older and younger parts of the Site 806

160   record (~16.4–14.1 Ma and ~13.3–12.3 Ma) were derived by assuming the same mean sedimentation rate as between ~14.1 Ma and ~13.3 Ma.

3 Results and discussion

3.1 Benthic foraminiferal $\delta^{18}O$ and $\delta^{13}C$ values

The isotope record of Site 747 (Fig. 2) displays features typical of middle Miocene sequences, including the stepped increase

165   in benthic $\delta^{18}O$ across the MMCT and the pronounced $\delta^{13}C$ maxima associated with the "Monterey" carbon isotope excursion (e.g., Holbourn et al., 2007, 2014; Kochhann et al., 2016; Vincent and Berger, 1985). From ~16.0 Ma to ~15.3 Ma, we analysed stable isotope compositions of both *C. mundulus* and *C. wuellerstorfi*, allowing for a direct assessment of species-specific effects on the isotopic compositions of these two different epifaunal species (Fig. 2a and c). $\delta^{18}O$ values

measured on *C. mundulus* and *C. wuellerstorfi* appear indistinguishable, whereas a consistent offset of up to ~0.5 ‰ exists

170 between the δ^{13}C values of these species at Site 747. Similar δ^{13}C offsets between *C. mundulus* and *C. wuellerstorfi* have been previously observed for the sub-Antarctic Atlantic during the Quaternary (Gottschalk et al., 2016). Our δ^{13}C values from the middle Miocene underscore the need to carefully examine inter-species offsets in δ^{13}C before combining different species to produce a single δ^{13}C curve.
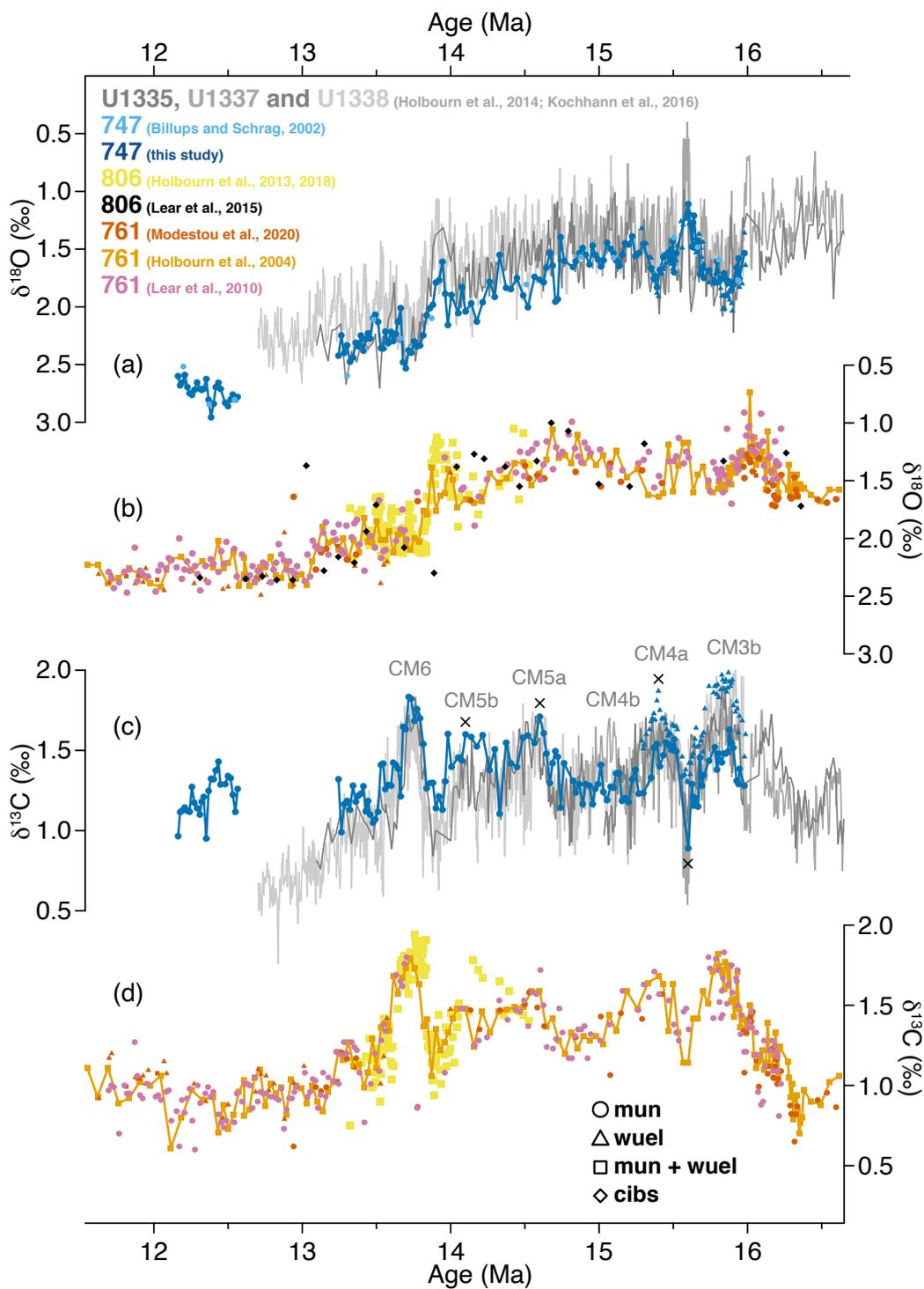
Fig. 2: Comparison of benthic isotope data. Benthic foraminiferal $\delta^{18}O$ (**a**, **b**) and $\delta^{13}C$ (**c**, **d**) records are shown from ODP Site 747 in the Southern Ocean (Billups and Schrag, 2002; this study), ODP Site 761 in the eastern Indian Ocean (Holbourn et al., 2004; Lear et al., 2010; Modestou et al., 2020), ODP Site 806 in the western equatorial Pacific (Holbourn et al., 2013, 2018; Lear et al., 2015) as well as IODP Sites U1335, U1337 and U1338 in the eastern equatorial Pacific Ocean (Holbourn et al., 2014; Kochhann et al., 2016). Correlation tie points for Site 747 (this study) are visualized with black crosses. We only plot $\delta^{18}O$ and $\delta^{13}C$ values from Sites 747 and 761 that were measured on the species *C. mundulus* (mun) and *C. wuellerstorfi* (wuel). In contrast to Site 747, offsets in both $\delta^{18}O$ and $\delta^{13}C$ between these species appear minimal at Site 761 (Holbourn et al., 2004). We note that we also use Δ_{47} values from other benthic foraminiferal species from Site 761 (see Modestou et al. (2020) for details), as no species-specific vital effects on benthic foraminiferal Δ_{47} have been observed (Modestou et al., 2020; Piasecki et al., 2019). For Site 806, we show $\delta^{18}O$ values of *Cibicidoides* spp. (cibs) (Lear et al., 2015), in addition to $\delta^{18}O$ and $\delta^{13}C$ measured specifically on tests of *C. mundulus* and *C. wuellerstorfi* (Holbourn et al., 2013, 2018). $\delta^{18}O$, $\delta^{13}C$ and Δ_{47} at Sites 747 and 761 were measured several times per sample in this study and Modestou et al. (2020). See Fig. S3 for Δ_{47} values and number of replicate measurements for each sediment sample.

3.2 Revised estimates of bottom water temperature for the middle Miocene

As expected, the Δ_{47} signal (Fig. S3a) is much noisier in comparison to $\delta^{18}O$ and $\delta^{13}C$ (Fig. 2), necessitating an averaging of Δ_{47} over many adjacent samples before interpreting the data in terms of calcification temperature. We have visualized our Δ_{47}-based BWT values for interpretation (Fig. 3a) using two different approaches: (1) To obtain the necessary precision, we averaged results from around 30–40 individual measurements from neighbouring samples, avoiding averaging across hiatuses and intervals with no measurements. These BWT averages are shown as filled circles, with horizontal lines indicating the averaging intervals and vertical lines indicating 68 % (solid) and 95 % (dashed) confidence intervals. The number of measurements used for the calculation of each mean temperature value is listed at the top of Fig. 3. (2) 400 kyr-moving averages based on 30 or more measurements are shown as solid lines, whereas those based on fewer measurements are dotted. The latter approach does not require a decision on each averaging interval, and thus may be better suited for inter-site comparison. We note that small-scale features in the moving average curves are likely caused by the scatter in the underlying individual Δ_{47} measurements, and should not be interpreted as real climate signals.

Independent of the averaging approach, Δ_{47}-based BWTs at Site 747 are highest (~8–10°C) from around 16.0 Ma to 14.5 Ma during the Miocene climatic optimum (MCO), and decrease thereafter by ~3–5°C (Fig. 3a). A transient warming (by ~2–4°C) starting between 13.5 Ma and 14 Ma is followed by a return to colder conditions from ~12.6 Ma to ~12.2 Ma. A hiatus prevents us from drawing any inferences about bottom water conditions from ~13.2 Ma to ~12.6 Ma.
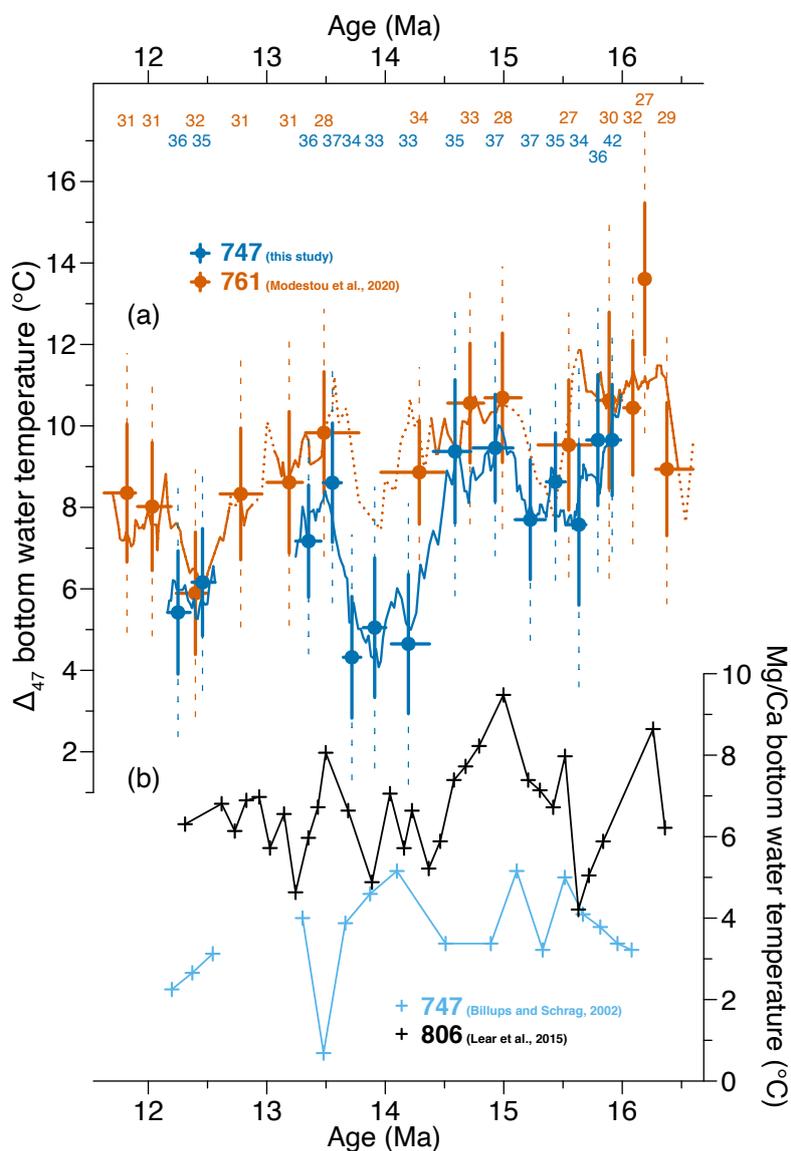
Fig. 3: Middle Miocene bottom water temperatures based on benthic foraminiferal Δ_{47} and Mg/Ca from ODP Sites 747, 761 and 806. (a) Δ_{47}-based temperatures based on averages of >30 Δ_{47} measurements each are shown as filled circles (horizontal solid lines: averaging intervals, vertical solid lines: 68 % confidence intervals, vertical dashed lines: 95 % confidence intervals). The number of measurements used for each average is shown at the top of the plot. The position on the x-axis shows the average age of each temperature value. 400 kyr-moving averages based on at least 30 and fewer than 30 measurements are shown as solid and dotted lines, respectively. Note that rapid fluctuations (of around 1°C) in these moving averages should not be interpreted in terms of climate (see Results and Discussion). (b) Mg/Ca temperatures from Site 747 are as published previously (Billups and Schrag, 2002). For Site 806, temperatures were calculated from infaunal foraminiferal Mg/Ca (Lear et al., 2015) using seawater Mg/Ca (polynomial curve fit through compiled seawater Mg/Ca records) and the favored linear temperature calibration of Lear et al. (2015).

215   Comparison of our Δ_{47}-based BWTs from Site 747 with Δ_{47}-based BWTs from Site 761 off northwest Australia in the Indian
       Ocean (Modestou et al., 2020) reveals good agreement, where temperatures are based on at least 30 Δ_{47} measurements (solid
       lines of the moving averages), with the Site 747 BWTs being slightly lower. Temperature averages from <30 measurements
       (dotted lines) are less certain, and thus not focus of our interpretation here (see Methods). Note that we processed the Δ_{47}
       measurement values from Site 761 (Modestou et al., 2020) in the same way as our results from Site 747 (e.g., temperature
220   calibration, smoothing) to optimize comparability of BWTs from these two middle Miocene reference sites. Similar absolute
       BWTs at Sites 747 and 761 during the Miocene may be expected from their similar present-day temperature ranges (~1–2°C;
       Fig. 1). Our study confirms the similarity of BWTs at these sites for large parts of the studied interval, suggesting a close to
       modern meridional temperature gradient around 2000 m water depth in a scenario of substantially (~3–9°C) warmer bottom
       waters. Unfortunately, the period of most pronounced BWT change at Site 747 is characterized by very low data density at
225   Site 761, due to low benthic foraminiferal abundances resulting in few measurements, and possibly a hiatus (core break
       between Cores 5H and 6H from Site 761 around 14.1 Ma). This leaves open the question whether the substantial cooling
       around 14.5–14.0 Ma and the subsequent warming were restricted to particular regions in the Southern Ocean, or whether
       they were more widespread features.

       Interestingly, a Mg/Ca record of the infaunal benthic foraminifer *O. umbonatus* from ODP Site 806 in the equatorial Pacific
230   (Lear et al., 2015) indicates BWT trends that are similar to those reconstructed from Δ_{47} at Site 747 during the MMCT
       (Fig. 3). Even though the Site 806 Mg/Ca record is of limited temporal resolution (~100–200 kyr), this low latitude record
       provides evidence that the early cooling and the subsequent warming reconstructed at Site 747 could have indeed been of
       global significance.

       Other available Mg/Ca-based BWT records covering the MMCT do not show the same features. Similar to Site 806, Mg/Ca
235   ratios were also measured on the infaunal species *O. umbonatus* at Site 761 (Lear et al., 2010). This approach yields BWTs
       that are within uncertainty of those from Δ_{47} measured at the same site (Fig. S4), regardless of whether or not the Mg/Ca-
       based BWTs have been corrected for changes in saturation state (Modestou et al., 2020). However, Mg/Ca-based BWT
       estimates from that site have been deemed less reliable than those from Site 806, due to unusual and variable pore water
       chemistry at Site 761 (Lear et al., 2015), and are compromised by reduced data density in crucial intervals (as noted above).
240   In comparison to Sites 761 and 806 where an infaunal foraminiferal species has been used (Lear et al., 2010, 2015), Mg/Ca
       records from Southern Ocean Sites 747 (Kerguelen Plateau) and 1171 (South Tasman Rise) were measured on the epifaunal
       species *C. mundulus* (Billups and Schrag, 2002; Shevenell et al., 2008). These Mg/Ca-based BWT records also do not show
       the same temperature pattern as our Δ_{47}-derived BWT record from Site 747 or the Mg/Ca-derived BWT record from Site 806
       (Fig. S4). The observed discrepancies suggest additional non-thermal controls on Mg/Ca and/or Δ_{47}, which may be related to
245   seawater chemistry during test precipitation and/or post-depositional alteration, such as dissolution.

Seawater chemistry does not appear to significantly influence Δ_{47} signatures in foraminifera over the range of natural variation (e.g., Tripati et al., 2015; Watkins and Hunt, 2015), whereas Mg/Ca signatures can be affected by changes in seawater Mg/Ca (Evans and Müller, 2012) and carbonate ion saturation (Elderfield et al., 2006; Yu and Elderfield, 2008). On the timescales considered here, the latter is more likely to be important. The relatively few Mg/Ca-based BWTs from

250   Site 747 can be directly compared to our BWTs based on Δ_{47} from the same site (Fig 4a). Δ_{47}- and Mg/Ca-based BWTs appear to diverge most pronouncedly in times of increased dissolution (high percentage of benthic foraminiferal tests and fragments) at Site 747, indicating fluctuations in bottom water carbonate ion saturation (Diester-Haass et al. (2013); Fig. 4b and c). Mg/Ca-based temperatures from Site 747 were measured on foraminiferal tests of the epifaunal species *C. mundulus*; compared to infaunal foraminifera, this species lives in more direct contact with bottom water, and may thus be more prone

255   to saturation state-related effects (Elderfield et al., 2006; Lear et al., 2015). The observation of diverging Mg/Ca- and Δ_{47}-based BWTs in times of increased dissolution supports the interpretation of a possible saturation state effect on the Mg/Ca signatures of *C. mundulus* (see Fig. S5 for sensitivity study). For Site 1171, we do not have constraints on saturation state variability.

In addition to saturation state effects, variable dissolution itself (Fig. 4b and c) could have influenced foraminiferal Mg/Ca

260   and/or Δ_{47} signatures. For planktic foraminifera, dissolution controlled by bottom water saturation has the potential to significantly lower initial Mg/Ca signatures and thus also the estimated ocean temperatures in certain burial settings (e.g., Regenberg et al., 2014). Dissolution may also impact the Mg/Ca signatures of benthic foraminiferal tests, although the tests of benthic foraminifera appear generally denser and more resistant to dissolution than those of planktic foraminifera (e.g., Berger, 1973; Pearson et al., 2001). The effects of dissolution on benthic foraminiferal Mg/Ca have thus received little

265   attention. Similarly, dissolution effects on benthic foraminiferal Δ_{47} signatures have not yet been specifically assessed. While there is currently no evidence for a significant dissolution effect on foraminiferal Δ_{47} (e.g., Breitenbach et al., 2018; Leutert et al., 2019) or variable dissolution of benthic foraminiferal calcite at Site 747 during the interval of this study (Fig. S2), a potential effect of dissolution cannot be fully ruled out. We interpret Δ_{47}-based temperatures as unaffected by dissolution in the absence of indications otherwise, but note that this aspect warrants further study.
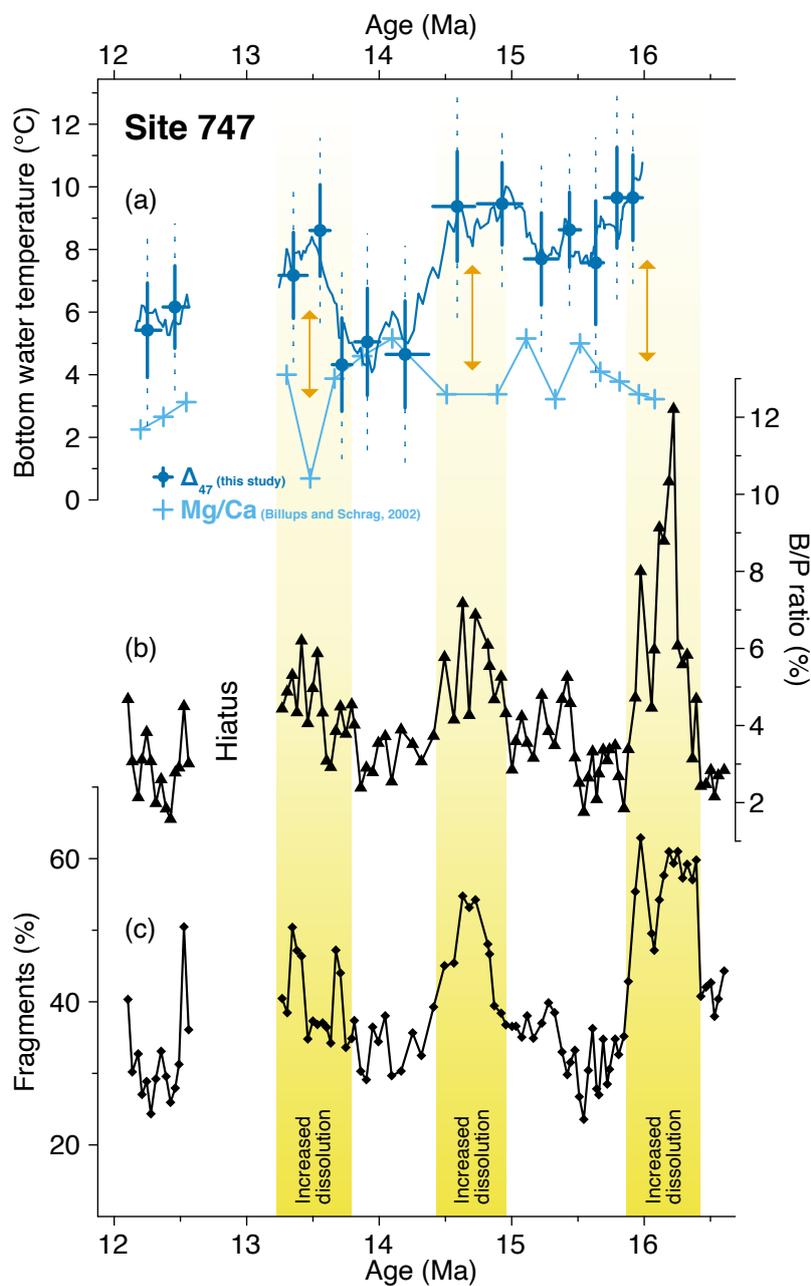
270

Fig. 4: Bottom water temperature and dissolution at Site 747. (**a**) Δ_{47}- and Mg/Ca-based BWT estimates (this study; Billups and Schrag, 2002) are shown versus (**b**) percent benthic to planktic (B/P) foraminiferal test ratios (Diester-Haass et al., 2013) and (**c**) percent fragments in a sample (Diester-Haass et al., 2013). Percent fragments and B/P foraminiferal test ratios have been previously used to monitor dissolution at Site 747 (Diester-Haass et al., 2013). Intervals interpreted as affected by increased dissolution of planktic foraminifera are highlighted with yellow bars. Orange arrows indicate intervals where Δ_{47}- and Mg/Ca-based temperature estimates appear to diverge most.

275

3.3 Regional and global implications

$\delta^{18}O_{bw}$ signatures have been widely used to infer the evolution of global ice volume during the Neogene (e.g., Billups and Schrag, 2002; Lear et al., 2010, 2015; Modestou et al., 2020; Shevenell et al., 2008). We calculated $\delta^{18}O_{bw}$ values from
280 measured benthic foraminiferal $\delta^{18}O$ in combination with Δ_{47}-based BWTs (Fig. 5e). Benthic foraminiferal $\delta^{18}O$ values of the taxon *Cibicidoides* were averaged over the same intervals as have been used for Δ_{47} averaging. For Site 747, we used the $\delta^{18}O$ values from this study (measured on *C. mundulus* and *C. wuellerstorfi*), whereas the foraminiferal $\delta^{18}O$ values for Site 761 were compiled from existing studies (Holbourn et al., 2004; Lear et al., 2010; Modestou et al., 2020). Due to comparably large random errors in our Δ_{47}-based BWT estimates, the propagated uncertainties in $\delta^{18}O_{bw}$ are also large.
285 However, systematic biases in our $\delta^{18}O_{bw}$ estimates may be smaller compared to other methods (e.g., paired benthic foraminiferal Mg/Ca and $\delta^{18}O$ measurements) because Δ_{47} signatures seem to be largely independent of complicating environmental parameters and/or foraminiferal vital effects (e.g., Leutert et al., 2019; Peral et al., 2018; Piasecki et al., 2019; Tripati et al., 2015; Watkins and Hunt, 2015). The earliest interval of this study (>15.6 Ma) is characterized by $\delta^{18}O_{bw}$ values ranging from approximately -0.1 ‰ to 1.3 ‰. For the later MCO (15.6–13.9 Ma), our estimates of $\delta^{18}O_{bw}$ range from around
290 -0.3 ‰ to 0.7 ‰, and increase to ~0.3–1.0 ‰ after the MMCT. All reconstructed $\delta^{18}O_{bw}$ values are consistently higher than expected for minimal ice (i.e. -0.89 ‰ according to Cramer et al. (2011)). Therefore, our results suggest the presence of substantial ice sheets on Antarctica throughout the warm MCO, similar to previous estimates of middle Miocene $\delta^{18}O_{bw}$ (e.g., Modestou et al., 2020). This interpretation is robust towards utilizing different suggested $\delta^{18}O$-temperature relationships (Fig. S6). However, we cannot exclude the presence of short-lived (orbital-scale) minima in global ice volume
295 during peak MCO interglacials (e.g., Levy et al., 2016), which may not be visible in the Δ_{47}-based records due to their temporal resolution.

Our Southern Ocean bottom water proxy record can be compared to evidence of past ice sheet variability from the Antarctic margin, in addition to orbital parameters. The stepped main increase in benthic $\delta^{18}O$ starting between 13.8 Ma and 14.0 Ma (Fig. 5d) is associated with growing ice sheets (increasing $\delta^{18}O_{bw}$, Fig. 5e) and occurs in an interval of low seasonal contrast
300 over Antarctica (declining eccentricity, decreasing amplitude variations in obliquity, Fig. 5a), as pointed out by Holbourn et al. (2005). The inferred ice volume increase recorded at Site 747 is supported by evidence for an episode of maximum ice sheet advance (MISA-4) recorded in the ANDRILL (AND)-2A drill core from the western Ross Sea, Antarctica (Levy et al., 2016). Similarly, an earlier period of maximum ice sheet advance documented in the Ross Sea around 14.7–14.6 Ma (MISA-3) corresponds to a maximum in $\delta^{18}O_{bw}$ at Site 747 (suggesting larger global ice volume). The early MCO is characterized by
305 several intervals of peak warmth at the ANDRILL Site (PW-3 to PW-5) (Levy et al., 2016). Unfortunately, this interval is not sufficiently covered by our Site 747 record to draw any conclusions; further proxy records are required to clarify the impact of Antarctic warming during the PW episodes on Southern Ocean bottom waters and at larger scales.
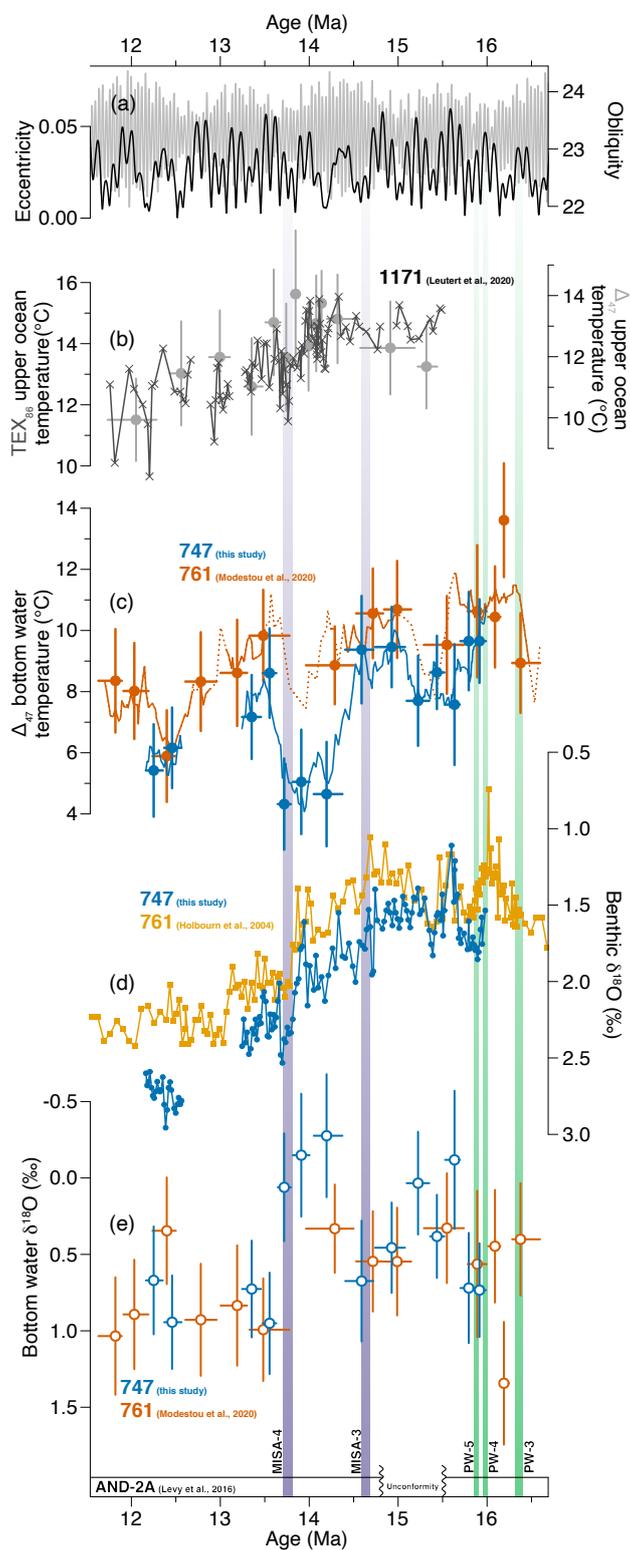
Fig. 5: Compilation of records for the MMCT. (**a**) Obliquity and eccentricity, (**b**) Δ_{47}- and TEX$_{86}$-based upper ocean temperatures from

310 ODP Site 1171 on the South Tasman Rise are shown with (**c**) Δ_{47}-based bottom water temperatures (BWTs), (**d**) benthic foraminiferal δ^{18}O and (**e**) bottom water δ^{18}O ($\delta^{18}O_{bw}$) from ODP Sites 747 and 761. In addition, we highlight distinct episodes of maximum ice sheet advance (MISA-3 and MISA-4, purple bars) and peak warmth (PW-3 to PW-5, green bars) around Antarctica derived from the ANDRILL (AND)-2A drill core (western Ross Sea; Levy et al., 2016). Δ_{47}-based BWTs (Modestou et al., 2020; this study) and upper ocean temperatures (Leutert et al., 2020) are shown with 68 % confidence intervals. TEX$_{86}$-based temperatures (Leutert et al., 2020) are

315 based on the subsurface calibration of Ho and Laepple (2016). Site 761 benthic δ^{18}O values are from Holbourn et al. (2004). Eccentricity and obliquity are from Laskar et al. (2004).

Our observations suggest a decoupling between global ice volume and BWT in the Southern Ocean (Fig. 5c–e). Significantly, the stepped increase in benthic foraminiferal δ^{18}O (and $\delta^{18}O_{bw}$) around 14.0–13.7 Ma (~0.5–1.0 ‰, interpreted

320 as cryosphere expansion) occurs clearly (roughly 0.5 Myr) later than the BWT drop. A similar decoupling of global ice volume and BWT was discussed based on the Mg/Ca record of Site 806 (Lear et al., 2015), and suggested to be related to feedbacks and thresholds controlling Antarctic ice growth. It is possible that the bottom water temperature signal at Site 747 reflects changes in Southern Ocean hydrography, which might also have been transferred to the deep Pacific. Majewski and Bohaty (2010) measured δ^{18}O on middle Miocene benthic (*Cibicidoides* spp.) and planktic foraminifera (e.g., *Globigerina*

325 *bulloides*) at Site 747 across the MMCT. These authors documented a marked increase in calculated δ^{18}O differences between *Cibicidoides* spp. and *G. bulloides* (vertical δ^{18}O gradient) during the main increase in δ^{18}O. While we cannot presently compare our Site 747 BWTs to upper ocean temperatures from the same site due to the lack of planktic foraminiferal Δ_{47} data, we compare our BWT record to Δ_{47}- and TEX$_{86}$-based upper ocean temperature records from Site 1171 located on the South Tasman Rise at slightly lower latitudes (Fig. 5b and c; Leutert et al. (2020)). Acknowledging

330 the caveat of substantial geographical distance between these sites, we find no evidence for a strengthening in the vertical temperature gradient at high southern latitudes at that time. To the contrary, the bottom water warming starting during or slightly after the stepped increase in global ice volume diminishes the temperature gradient. Therefore, we relate the observed increase in the vertical δ^{18}O gradient at Site 747 primarily to a freshening of the upper ocean water column relative to bottom waters associated with Antarctic ice sheet expansion, in line with the interpretation of Majewski and Bohaty

335 (2010). An upper ocean freshening across the MMCT was also reconstructed at Site 1171 (Leutert et al., 2020). At high southern latitudes, salinity has a large effect on stratification (e.g., Kuhnert et al., 2009). Similar to Leutert et al. (2020), we hypothesize that a Southern Ocean freshening concurrent with Antarctic ice sheet expansion may have decreased convective vertical mixing resulting in a shielding of upper ocean waters from comparably warm deeper waters. This stratification mechanism may have influenced Southern Ocean BWTs during the MMCT, explaining the transient bottom water warming

340 and the partially opposing trends of upper ocean temperature and BWT. An increase in stratification starting between 13.5 Ma and 14 Ma is supported by an increase in dissolution at that time (Figs. 4 and S5), which may be related to reduced ventilation and an increase in CO_2 storage in the deep ocean.

4 Conclusions

We constrain the middle Miocene BWT evolution at Site 747 in the Southern Ocean with clumped isotope thermometry.
345   Similar to existing BWT reconstructions from lower latitude sites, we find that Southern Ocean BWTs were substantially warmer than today, despite the presence of ice sheets on Antarctica. The observed discrepancies between Δ_{47}- and Mg/Ca-based BWTs may be caused by changes in deep water carbonate ion saturation, but further Mg/Ca and Δ_{47} measurements are needed to conclusively test this hypothesis. We cannot fully rule out a dissolution effect on benthic foraminiferal Δ_{47}, although there is currently no evidence for such an effect. Taken at face value, our Δ_{47} values indicate pronounced shifts in
350   Southern Ocean BWTs, which resemble observations at equatorial Pacific Site 806, and a long-term decrease of ~3–5°C across the MMCT. Comparison of changes in BWT and $\delta^{18}O_{bw}$ indicates a significant degree of decoupling and a more complicated sequence of events surrounding the MMCT than previously appreciated based on benthic $\delta^{18}O$ alone. These findings suggest the involvement of additional feedbacks and thresholds in middle Miocene ice growth and/or regional effects on middle Miocene BWTs at Site 747. We hypothesize that a possible factor could be shifts in the vertical density
355   structure of the Southern Ocean. Reconstructed BWTs may in part reflect changes in heat transport between upper and deep ocean, induced by growing ice sheets on Antarctica. Independent higher-resolution BWT records from additional locations in and outside the Southern Ocean would allow for examining the spatial scale of the changes observed at Site 747 as a basis for better understanding the drivers of the MMCT.

Appendix A: Clumped isotope methodological details

360   Clumped isotope data are presented in the conventional Δ_{47} notation, which is defined as follows (e.g., Eiler, 2007; Huntington et al., 2009):

$$\Delta_{47}\ (‰)\ =\ [(\frac{R^{47}}{R^{47*}}-1)-(\frac{R^{46}}{R^{46*}}-1)-(\frac{R^{45}}{R^{45*}}-1)]\times 1000 \qquad (A1)$$

365   R^{i} are the measured abundance ratios of mass i relative to mass 44. R^{i*} represent the stochastic abundance ratios calculated from the bulk isotope composition of the sample ($\delta^{18}O$ and $\delta^{13}C$).

All (clumped) isotope measurements were carried out in micro-volume mode. At the University of Bergen (UiB), we followed the long-integration dual-inlet (LIDI) protocol (Hu et al., 2014; Müller et al., 2017), whereas the measurements at ETH Zurich were performed via repeated cycles of alternating reference and sample gas measurements (Meckler et al., 2014;
370   Rodríguez-Sanz et al., 2017). For data processing, we used the community software "Easotope" (John and Bowen, 2016). The different steps for calculating the final Δ_{47} values include a pressure-sensitive baseline correction (Bernasconi et al.,

2013; He et al., 2012; Meckler et al., 2014) and a conversion into the absolute reference frame (Dennis et al., 2011). For the conversion into the absolute reference frame, we utilized replicate measurements of three (UiB) respectively four (ETH Zurich) different correction standards from a window of ±12–40 standards around the sample replicate. At UiB, we used the carbonate standards ETH-1, ETH-3 and ETH-4 for correction from October 2016 to December 2016; ETH-2 was used for monitoring during this interval. From August 2018 to June 2019, ETH-1, ETH-2 and ETH-3 were used for correction and ETH-4 for monitoring. For the measurements carried out at ETH Zurich, ETH-1, ETH-2, ETH-3 and ETH-4 were all included in the correction procedure. The accepted ETH standard values are from Bernasconi et al. (2018). These ETH standard values were determined using an acid fractionation correction of +0.062 ‰ (Defliese et al., 2015). Measured $\delta^{18}O$ and $\delta^{13}C$ values were drift-corrected based on three (UiB) respectively four (ETH Zurich) different correction standards (with scale "stretching" only applied for $\delta^{18}O$ at UiB and for both $\delta^{18}O$ and $\delta^{13}C$ at ETH). All isotope data were calculated with the Brand correction parameters (Daëron et al., 2016). Further details on analytical and data processing methods can be found elsewhere (Leutert et al., 2019; Piasecki et al., 2019).

We excluded three clumped isotope measurements as outliers, based on their offset of more than four standard deviations (4×0.037 ‰, estimated from the long-term mean reproducibility of all standards) from the mean. Raw standard and sample measurement data are included in the supplement and will be available on EarthChem at the time of publication.

Data availability

The data from this paper are archived in the supplement. In addition, the final temperature data will be published at Pangaea (https://doi.pangaea.de/10.1594/PANGAEA.923258) and the full raw data on the EarthChem Database (a link to the EarthChem dataset will be provided prior to publication).

Author contribution

T.J.L. and A.N.M. initiated and designed the study. T.J.L. generated and analysed clumped isotope data under the oversight of A.N.M., S.M. and S.M.B. All the authors contributed to the palaeoceanographic interpretation. T.J.L. wrote the paper with contributions from A.N.M., S.M. and S.M.B.

Competing interests

The authors declare that they have no conflict of interest.

Acknowledgements

We thank Enver Alagoz and Inigo Müller for analytical support, Janika Jöhnck for insightful discussions and all authors who shared their published data. This research used data and samples provided by the Ocean Drilling Program (ODP) and the
400   International Ocean Discovery Program (IODP), sponsored by the US National Science Foundation (NSF) and participating countries. Funding for the research was provided by the European Research Council (ERC) under the European Union's Horizon 2020 research and innovation programme (grant agreement No 638467) and by the Trond Mohn Foundation.

References

Abrajevitch, A., Roberts, A. P. and Kodama, K.: Volcanic iron fertilization of primary productivity at Kerguelen Plateau,
405   Southern Ocean, through the Middle Miocene Climate Transition, Palaeogeogr. Palaeoclimatol. Palaeoecol., 410, 1–13, doi:10.1016/j.palaeo.2014.05.028, 2014.

Belkin, I. M. and Gordon, A. L.: Southern Ocean fronts from the Greenwich meridian to Tasmania, J. Geophys. Res., 101(C2), 3675–3696, doi:10.1029/95jc02750, 1996.

Berger, W. H.: Deep-Sea Carbonates: Pleistocene Dissolution Cycles, J. Foraminifer. Res., 3(4), 187–195,
410   doi:10.2113/gsjfr.3.4.187, 1973.

Bernasconi, S. M., Hu, B., Wacker, U., Fiebig, J., Breitenbach, S. F. M. and Rutz, T.: Background effects on Faraday collectors in gas-source mass spectrometry and implications for clumped isotope measurements, Rapid Commun. Mass Spectrom., 27(5), 603–612, doi:10.1002/rcm.6490, 2013.

Bernasconi, S. M., Müller, I. A., Bergmann, K. D., Breitenbach, S. F. M., Fernandez, A., Hodell, D. A., Jaggi, M., Meckler,
415   A. N., Millan, I. and Ziegler, M.: Reducing uncertainties in carbonate clumped isotope analysis through consistent carbonate-based standardization, Geochemistry, Geophys. Geosystems, 19, 2895–2914, doi:10.1029/2017GC007385, 2018.

Billups, K. and Schrag, D. P.: Paleotemperatures and ice volume of the past 27 Myr revisited with paired Mg/Ca and $^{18}O/^{16}O$ measurements on benthic foraminifera, Paleoceanography, 17(1), 3–11, doi:10.1029/2000PA000567, 2002.

de Boer, B., van de Wal, R. S. W., Bintanja, R., Lourens, L. J. and Tuenter, E.: Cenozoic global ice-volume and temperature
420   simulations with 1-D ice-sheet models forced by benthic $\delta^{18}O$ records, Ann. Glaciol., 51(55), 23–33, doi:10.3189/172756410791392736, 2010.

Breitenbach, S. F. M., Mleneck-Vautravers, M. J., Grauel, A.-L., Lo, L., Bernasconi, S. M., Müller, I. A., Rolfe, J., Gázquez,

F., Greaves, M. and Hodell, D. A.: Coupled Mg/Ca and clumped isotope analyses of foraminifera provide consistent water temperatures, Geochim. Cosmochim. Acta, 236, 283–296, doi:10.1016/j.gca.2018.03.010, 2018.

425 Cramer, B. S., Miller, K. G., Barrett, P. J. and Wright, J. D.: Late Cretaceous-Neogene trends in deep ocean temperature and continental ice volume: Reconciling records of benthic foraminiferal geochemistry (δ^{18}O and Mg/Ca) with sea level history, J. Geophys. Res., 116, 1–23, doi:10.1029/2011jc007255, 2011.

Daëron, M., Blamart, D., Peral, M. and Affek, H. P.: Absolute isotopic abundance ratios and the accuracy of Δ_{47} measurements, Chem. Geol., 442, 83–96, doi:10.1016/j.chemgeo.2016.08.014, 2016.

430 Defliese, W. F., Hren, M. T. and Lohmann, K. C.: Compositional and temperature effects of phosphoric acid fractionation on Δ_{47} analysis and implications for discrepant calibrations, Chem. Geol., 396, 51–60, doi:10.1016/j.chemgeo.2014.12.018, 2015.

Dennis, K. J., Affek, H. P., Passey, B. H., Schrag, D. P. and Eiler, J. M.: Defining an absolute reference frame for 'clumped' isotope studies of CO_2, Geochim. Cosmochim. Acta, 75(22), 7117–7131, doi:10.1016/j.gca.2011.09.025, 2011.

435 Diester-Haass, L., Billups, K., Jacquemin, I., Emeis, K. C., Lefebvre, V. and Francois, L.: Paleoproductivity during the middle Miocene carbon isotope events: A data-model approach, Paleoceanography, 28(2), 334–346, doi:10.1002/palo.20033, 2013.

Eiler, J. M.: "Clumped-isotope" geochemistry—The study of naturally-occurring, multiply-substituted isotopologues, Earth Planet. Sci. Lett., 262(3–4), 309–327, doi:10.1016/j.epsl.2007.08.020, 2007.

440 Eiler, J. M.: Paleoclimate reconstruction using carbonate clumped isotope thermometry, Quat. Sci. Rev., 30(25–26), 3575–3588, doi:10.1016/j.quascirev.2011.09.001, 2011.

Elderfield, H., Yu, J., Anand, P., Kiefer, T. and Nyland, B.: Calibrations for benthic foraminiferal Mg/Ca paleothermometry and the carbonate ion hypothesis, Earth Planet. Sci. Lett., 250(3–4), 633–649, doi:10.1016/j.epsl.2006.07.041, 2006.

Evans, D. and Müller, W.: Deep time foraminifera Mg/Ca paleothermometry: Nonlinear correction for secular change in 445 seawater Mg/Ca, Paleoceanography, 27, 1–11, doi:10.1029/2012pa002315, 2012.

Fairbanks, R. G. and Matthews, R. K.: The marine oxygen isotope record in Pleistocene coral, Barbados, West Indies, Quat. Res., 10(2), 181–196, doi:10.1016/0033-5894(78)90100-X, 1978.

Fernandez, A., Müller, I. A., Rodriguez-Sanz, L., van Dijk, J., Looser, N. and Bernasconi, S. M.: A Reassessment of the

Precision of Carbonate Clumped Isotope Measurements: Implications for Calibrations and Paleoclimate Reconstructions,
450 Geochemistry Geophys. Geosystems, 18(12), 4375–4386, doi:10.1002/2017gc007106, 2017.

Flower, B. P. and Kennett, J. P.: Middle Miocene Ocean-Climate Transition - High-Resolution Oxygen and Carbon Isotopic Records from Deep-Sea Drilling Project Site 588A, Southwest Pacific, Paleoceanography, 8(6), 811–843, doi:10.1029/93pa02196, 1993.

Frigola, A., Prange, M. and Schulz, M.: Boundary conditions for the Middle Miocene Climate Transition (MMCT v1.0),
455 Geosci. Model Dev., 11(4), 1607–1626, doi:10.5194/gmd-11-1607-2018, 2018.

Ghosh, P., Adkins, J., Affek, H., Balta, B., Guo, W., Schauble, E. A., Schrag, D. and Eiler, J. M.: ^{13}C-^{18}O bonds in carbonate minerals: A new kind of paleothermometer, Geochim. Cosmochim. Acta, 70(6), 1439–1456, doi:10.1016/j.gca.2005.11.014, 2006.

Gottschalk, J., Riveiros, N. V, Waelbroeck, C., Skinner, L. C., Michel, E., Duplessy, J. C., Hodell, D. and Mackensen, A.:
460 Carbon isotope offsets between benthic foraminifer species of the genus Cibicides (Cibicidoides) in the glacial sub-Antarctic Atlantic, Paleoceanography, 31(12), 1583–1602, doi:10.1002/2016pa003029, 2016.

Gradstein, F. M., Ogg, J. G., Schmitz, M. and Ogg, G.: The Geologic Time Scale 2012, Elsevier, Oxford., 2012.

Grauel, A. L., Schmid, T. W., Hu, B., Bergami, C., Capotondi, L., Zhou, L. and Bernasconi, S. M.: Calibration and application of the 'clumped isotope' thermometer to foraminifera for high resolution climate reconstructions, Geochim.
465 Cosmochim. Acta, 108, 125–140, doi:10.1016/j.gca.2012.12.049, 2013.

He, B., Olack, G. A. and Colman, A. S.: Pressure baseline correction and high-precision CO_2 clumped-isotope (Δ_{47}) measurements in bellows and micro-volume modes, Rapid Commun. Mass Spectrom., 26(24), 2837–2853, doi:10.1002/rcm.6436, 2012.

Ho, S. L. and Laepple, T.: Flat meridional temperature gradient in the early Eocene in the subsurface rather than surface
470 ocean, Nat. Geosci., 9(8), 606–610, doi:10.1038/ngeo2763, 2016.

Holbourn, A., Kuhnt, W., Simo, J. A. and Li, Q.: Middle Miocene isotope stratigraphy and paleoceanographic evolution of the northwest and southwest Australian margins (Wombat Plateau and Great Australian Bight), Palaeogeogr. Palaeoclimatol. Palaeoecol., 208(1–2), 1–22, doi:10.1016/j.palaeo.2004.02.003, 2004.

Holbourn, A., Kuhnt, W., Schulz, M. and Erlenkeuser, H.: Impacts of orbital forcing and atmospheric carbon dioxide on
475 Miocene ice-sheet expansion, Nature, 438(7067), 483–487, doi:10.1038/nature04123, 2005.

Holbourn, A., Kuhnt, W., Schulz, M., Flores, J. A. and Andersen, N.: Orbitally-paced climate evolution during the middle Miocene "Monterey" carbon-isotope excursion, Earth Planet. Sci. Lett., 261(3–4), 534–550, doi:10.1016/j.epsl.2007.07.026, 2007.

Holbourn, A., Kuhnt, W., Frank, M. and Haley, B. A.: Changes in Pacific Ocean circulation following the Miocene onset of permanent Antarctic ice cover, Earth Planet. Sci. Lett., 365, 38–50, doi:10.1016/j.epsl.2013.01.020, 2013.

Holbourn, A., Kuhnt, W., Lyle, M., Schneider, L., Romero, O. and Andersen, N.: Middle Miocene climate cooling linked to intensification of eastern equatorial Pacific upwelling, Geology, 42(1), 19–22, doi:10.1130/G34890.1, 2014.

Holbourn, A., Kuhnt, W., Frank, M. and Haley, B.: Middle Miocene benthic oxygen and carbon stable isotopes of ODP Site 130-806B, Pangaea, doi:10.1594/PANGAEA.895208, 2018.

Hu, B., Radke, J., Schlüter, H. J., Heine, F. T., Zhou, L. and Bernasconi, S. M.: A modified procedure for gas-source isotope ratio mass spectrometry: the long-integration dual-inlet (LIDI) methodology and implications for clumped isotope measurements, Rapid Commun. Mass Spectrom., 28(13), 1413–1425, doi:10.1002/rcm.6909, 2014.

Huntington, K. W., Eiler, J. M., Affek, H. P., Guo, W., Bonifacie, M., Yeung, L. Y., Thiagarajan, N., Passey, B. H., Tripati, A. K., Daeron, M. and Came, R.: Methods and limitations of 'clumped' CO_2 isotope (Δ_{47}) analysis by gas-source isotope ratio mass spectrometry, J. Mass Spectrom., 44(9), 1318–1329, doi:10.1002/jms.1614, 2009.

John, C. M. and Bowen, D.: Community software for challenging isotope analysis: First applications of 'Easotope' to clumped isotopes, Rapid Commun. Mass Spectrom., 30(21), 2285–2300, doi:10.1002/rcm.7720, 2016.

Kele, S., Breitenbach, S. F. M., Capezzuoli, E., Meckler, A. N., Ziegler, M., Millan, I. M., Kluge, T., Deák, J., Hanselmann, K., John, C. M., Yan, H., Liu, Z. and Bernasconi, S. M.: Temperature dependence of oxygen- and clumped isotope fractionation in carbonates: A study of travertines and tufas in the 6–95 °C temperature range, Geochim. Cosmochim. Acta, 168, 172–192, doi:10.1016/j.gca.2015.06.032, 2015.

Kochhann, K. G. D., Holbourn, A., Kuhnt, W., Channell, J. E. T., Lyle, M., Shackford, J. K., Wilkens, R. H. and Andersen, N.: Eccentricity pacing of eastern equatorial Pacific carbonate dissolution cycles during the Miocene Climatic Optimum, Paleoceanography, 31, 1–17, doi:10.1002/2016PA002988, 2016.

Kominz, M. A., Browning, J. V, Miller, K. G., Sugarman, P. J., Mizintseva, S. and Scotese, C. R.: Late Cretaceous to Miocene sea-level estimates from the New Jersey and Delaware coastal plain coreholes: an error analysis, Basin Res., 20(2), 211–226, doi:10.1111/j.1365-2117.2008.00354.x, 2008.

Kuhnert, H., Bickert, T. and Paulsen, H.: Southern Ocean frontal system changes precede Antarctic ice sheet growth during the middle Miocene, Earth Planet. Sci. Lett., 284(3–4), 630–638, doi:10.1016/j.epsl.2009.05.030, 2009.

505   Langebroek, P. M., Paul, A. and Schulz, M.: Antarctic ice-sheet response to atmospheric CO_2 and insolation in the Middle Miocene, Clim. Past, 5(4), 633–646, doi:10.5194/cp-5-633-2009, 2009.

Laskar, J., Robutel, P., Joutel, F., Gastineau, M., Correia, A. C. M. and Levrard, B.: A long-term numerical solution for the insolation quantities of the Earth, Astron. Astrophys., 428(1), 261–285, doi:10.1051/0004-6361:20041335, 2004.

Lear, C. H., Rosenthal, Y. and Slowey, N.: Benthic foraminiferal Mg/Ca-paleothermometry: A revised core-top calibration,
510   Geochim. Cosmochim. Acta, 66(19), 3375–3387, doi:10.1016/s0016-7037(02)00941-9, 2002.

Lear, C. H., Mawbey, E. M. and Rosenthal, Y.: Cenozoic benthic foraminiferal Mg/Ca and Li/Ca records: Toward unlocking temperatures and saturation states, Paleoceanography, 25, 1–11, doi:10.1029/2009PA001880, 2010.

Lear, C. H., Coxall, H. K., Foster, G. L., Lunt, D. J., Mawbey, E. M., Rosenthal, Y., Sosdian, S. M., Thomas, E. and Wilson, P. A.: Neogene ice volume and ocean temperatures: Insights from infaunal foraminiferal Mg/Ca paleothermometry,
515   Paleoceanography, 30, 1437–1454, doi:10.1002/2015PA002833, 2015.

Leutert, T. J., Sexton, P. F., Tripati, A., Piasecki, A., Ho, S. L. and Meckler, A. N.: Sensitivity of clumped isotope temperatures in fossil benthic and planktic foraminifera to diagenetic alteration, Geochim. Cosmochim. Acta, 257, 354–372, doi:10.1016/j.gca.2019.05.005, 2019.

Leutert, T. J., Auderset, A., Martínez-García, A., Modestou, S. and Meckler, A. N.: Coupled Southern Ocean cooling and
520   Antarctic ice sheet expansion during the middle Miocene, Nat. Geosci., 13(9), 634–639, doi:10.1038/s41561-020-0623-0, 2020.

Levy, R., Harwood, D., Florindo, F., Sangiorgi, F., Tripati, R., von Eynatten, H., Gasson, E., Kuhn, G., Tripati, A., DeConto, R., Fielding, C., Field, B., Golledge, N., McKay, R., Naish, T., Olney, M., Pollard, D., Schouten, S., Talarico, F., Warny, S., Willmott, V., Acton, G., Panter, K., Paulsen, T., Taviani, M. and SMS Science Team: Antarctic ice sheet sensitivity to
525   atmospheric CO_2 variations in the early to mid-Miocene, Proc. Natl. Acad. Sci., doi:10.1073/pnas.1516030113, 2016.

Lewis, A. R., Marchant, D. R., Ashworth, A. C., Hemming, S. R. and Machlus, M. L.: Major middle Miocene global climate change: Evidence from East Antarctica and the Transantarctic Mountains, Geol. Soc. Am. Bull., 119(11–12), 1449–1461, doi:10.1130/0016-7606(2007)119[1449:Mmmgcc]2.0.Co;2, 2007.

Locarnini, R. A., Mishonov, A. V, Antonov, J. I., Boyer, T. P., Garcia, H. E., Baranova, O. K., Zweng, M. M., Paver, C. R.,

530   Reagan, J. R., Johnson, D. R., Hamilton, M. and Seidov, D.: World Ocean Atlas 2013, Volume 1: Temperature. S. Levitus, Ed., A. Mishonov Technical Ed., NOAA Atlas NESDIS 73, 40, 2013.

Majewski, W. and Bohaty, S. M.: Surface-water cooling and salinity decrease during the Middle Miocene climate transition at Southern Ocean ODP Site 747 (Kerguelen Plateau), Mar. Micropaleontol., 74(1–2), 1–14, doi:10.1016/j.marmicro.2009.10.002, 2010.

535   Marchitto, T. M., Curry, W. B., Lynch-Stieglitz, J., Bryan, S. P., Cobb, K. M. and Lund, D. C.: Improved oxygen isotope temperature calibrations for cosmopolitan benthic foraminifera, Geochim. Cosmochim. Acta, 130, 1–11, doi:10.1016/j.gca.2013.12.034, 2014.

Meckler, A. N., Ziegler, M., Millan, M. I., Breitenbach, S. F. M. and Bernasconi, S. M.: Long-term performance of the Kiel carbonate device with a new correction scheme for clumped isotope measurements, Rapid Commun. Mass Spectrom.,
540   28(15), 1705–1715, doi:10.1002/rcm.6949, 2014.

Meinicke, N., Ho, S. L., Hannisdal, B., Nürnberg, D., Tripati, A., Schiebel, R. and Meckler, A. N.: A robust calibration of the clumped isotopes to temperature relationship for foraminifers, Geochim. Cosmochim. Acta, 270, 160–183, doi:10.1016/j.gca.2019.11.022, 2020.

Modestou, S. E., Leutert, T. J., Fernandez, A., Lear, C. H. and Meckler, A. N.: Warm middle Miocene Indian Ocean bottom
545   water temperatures: comparison of clumped isotope and Mg/Ca based estimates, Paleoceanogr. Paleoclimatology, 35(11), doi:10.1029/2020PA003927, 2020.

Müller, I. A., Fernandez, A., Radke, J., van Dijk, J., Bowen, D., Schwieters, J. and Bernasconi, S. M.: Carbonate clumped isotope analyses with the long-integration dual-inlet (LIDI) workflow: scratching at the lower sample weight boundaries, Rapid Commun. Mass Spectrom., 31(12), 1057–1066, doi:10.1002/rcm.7878, 2017.

550   Pearson, P. N., Ditchfield, P. W., Singano, J., Harcourt-Brown, K. G., Nicholas, C. J., Olsson, R. K., Shackleton, N. J. and Hall, M. A.: Warm tropical sea surface temperatures in the Late Cretaceous and Eocene epochs, Nature, 414(6862), 481–487, doi:10.1038/35106617, 2001.

Peral, M., Daëron, M., Blamart, D., Bassinot, F., Dewilde, F., Smialkowski, N., Isguder, G., Bonnin, J., Jorissen, F., Kissel, C., Michel, E., Vázquez Riveiros, N. and Waelbroeck, C.: Updated calibration of the clumped isotope thermometer in
555   planktonic and benthic foraminifera, Geochim. Cosmochim. Acta, 239, 1–16, doi:10.1016/j.gca.2018.07.016, 2018.

Piasecki, A., Bernasconi, S. M., Grauel, A.-L., Hannisdal, B., Ho, S. L., Leutert, T. J., Marchitto, T. M., Meinicke, N.,

Tisserand, A. and Meckler, N.: Application of Clumped Isotope Thermometry to Benthic Foraminifera, Geochemistry, Geophys. Geosystems, 20(4), 1–9, doi:10.1029/2018GC007961, 2019.

Regenberg, M., Regenberg, A., Garbe-Schonberg, D. and Lea, D. W.: Global dissolution effects on planktonic foraminiferal
560   Mg/Ca ratios controlled by the calcite-saturation state of bottom waters, Paleoceanography, 29(3), 127–142, doi:10.1002/2013pa002492, 2014.

Rodríguez-Sanz, L., Bernasconi, S. M., Marino, G., Heslop, D., Müller, I. A., Fernandez, A., Grant, K. M. and Rohling, E. J.: Penultimate deglacial warming across the Mediterranean Sea revealed by clumped isotopes in foraminifera, Sci. Rep., 7, 1–11, doi:10.1038/s41598-017-16528-6, 2017.

565   Schauble, E. A., Ghosh, P. and Eiler, J. M.: Preferential formation of ^{13}C-^{18}O bonds in carbonate minerals, estimated using first-principles lattice dynamics, Geochim. Cosmochim. Acta, 70(10), 2510–2529, doi:10.1016/j.gca.2006.02.011, 2006.

Schlich, R., Wise, S. W. and the Expedition 120 Scientists: Site 747, in Proceedings of the Ocean Drilling Program, Initial Reports, 120, pp. 89–156., 1989.

Schlitzer, R.: Ocean Data View, [online] Available from: https://odv.awi.de, 2019.

570   Schmid, T. W. and Bernasconi, S. M.: An automated method for 'clumped-isotope' measurements on small carbonate samples, Rapid Commun. Mass Spectrom., 24(14), 1955–1963, doi:10.1002/rcm.4598, 2010.

Schmid, T. W., Radke, J. and Bernasconi, S. M.: Clumped-isotope measurements on small carbonate samples with a Kiel IV carbonate device and a MAT 253 mass spectrometer, Thermo Fish. Appl. Note, (30233), 2012.

Shevenell, A. E., Kennett, J. P. and Lea, D. W.: Middle Miocene ice sheet dynamics, deep-sea temperatures, and carbon
575   cycling: A Southern Ocean perspective, Geochemistry Geophys. Geosystems, 9, 1–14, doi:10.1029/2007GC001736, 2008.

Sosdian, S. M., Greenop, R., Hain, M. P., Foster, G. L., Pearson, P. N. and Lear, C. H.: Constraining the evolution of Neogene ocean carbonate chemistry using the boron isotope pH proxy, Earth Planet. Sci. Lett., 498, 362–376, doi:10.1016/j.epsl.2018.06.017, 2018.

Super, J. R., Thomas, E., Pagani, M., Huber, M., O'Brien, C. and Hull, P. M.: North Atlantic temperature and pCO$_2$ coupling
580   in the early-middle Miocene, Geology, 46(6), 519–522, doi:10.1130/g40228.1, 2018.

Tripati, A. K., Eagle, R. A., Thiagarajan, N., Gagnon, A. C., Bauch, H., Halloran, P. R. and Eiler, J. M.: ^{13}C-^{18}O isotope signatures and "clumped isotope" thermometry in foraminifera and coccoliths, Geochim. Cosmochim. Acta, 74(20), 5697–

5717, doi:10.1016/j.gca.2010.07.006, 2010.

Tripati, A. K., Hill, P. S., Eagle, R. A., Mosenfelder, J. L., Tang, J., Schauble, E. A., Eiler, J. M., Zeebe, R. E., Uchikawa, J.,
585 Coplen, T. B., Ries, J. B. and Henry, D.: Beyond temperature: Clumped isotope signatures in dissolved inorganic carbon
species and the influence of solution chemistry on carbonate mineral composition, Geochim. Cosmochim. Acta, 166, 344–
371, doi:10.1016/j.gca.2015.06.021, 2015.

Vincent, E. and Berger, W. H.: Carbon Dioxide and Polar Cooling in the Miocene: The Monterey Hypothesis, in The Carbon
Cycle and Atmospheric CO2: Natural Variations Archean to Present, vol. 32, edited by E. T. Sundquist and W. S. Broecker,
590 pp. 455–468, AGU, Washington, D. C., 1985.

Watkins, J. M. and Hunt, J. D.: A process-based model for non-equilibrium clumped isotope effects in carbonates, Earth
Planet. Sci. Lett., 432, 152–165, doi:10.1016/j.epsl.2015.09.042, 2015.

Yu, J. M. and Elderfield, H.: Mg/Ca in the benthic foraminifera Cibicidoides wuellerstorfi and Cibicidoides mundulus:
Temperature versus carbonate ion saturation, Earth Planet. Sci. Lett., 276(1–2), 129–139, doi:10.1016/j.epsl.2008.09.015,
595 2008.

Zachos, J. C., Pagani, M., Sloan, L., Thomas, E. and Billups, K.: Trends, rhythms, and aberrations in global climate 65 Ma to
present, Science, 292, 686–693, doi:10.1126/science.1059412, 2001.